PHYSICAL REVIEW B VOLUME 52, NUMBER 11 15 SEPTEMBER 1995-I

Magnetization of graphene tubules

M. F. Lin and Kenneth W.-K. Shung

Physics Department, National Tsing Hua University, Hsinchu, Taiwan 30043, The Republic of China

(Received 9 January 1995; revised manuscript received 3 April 1995)

Magnetization (M) comes from both the persistent currents and the spin polarization. The spin-B interaction is important in a graphene tubule, because it makes the one-dimensional subband with the divergent density of states capable of crossing the Fermi level ($E_F=0$ eV). It causes cusps in magnetization and power divergencies in differential susceptibility (χ_M), and destroys the periodicity (period $\phi_0=hc/e$) of the physical properties. The special structures shown in M and χ_M are found to be insensitive to the chirality. The power divergencies in χ_M are replaced by the peak structures at low temperature (T). The order of χ_M is 10^{-4}–10^{-5}; therefore, the peak structures are measurable at $T\leq 1$ K. The temperature effect in reducing magnetization is relatively obvious for a larger semiconducting tubule. Moreover, the anomalous temperature effect due to the spin-B interaction exists in all the metallic tubules at the relatively low T. For the doped graphene tubule, M and χ_M exhibit more special structures, since both the electronic structure and the finite Fermi level vary with ϕ simultaneously. The magnetic response is enhanced by the doping, and it is relatively strong for a larger tubule. The magnetism at the small flux is possibly altered from paramagnetism (diamagnetism) to diamagnetism (paramagnetism) by varying the free-carrier density.

I. INTRODUCTION

Iijima[1] recently reported observation of coaxial tubules made up of graphite carbons. Each graphene tubule is just a graphite sheet which is rolled up in cylindrical form. Its radius is only between 10 and 150 Å. Graphene tubules represent an interesting class of quasi-one-dimensional (1D) system. Due to their cylindrical symmetry and nanoscaled size, they have attracted many recent studies.[2–10] Among these studies, abundant single-shell tubules could be produced in large-scale synthesis, and their radii could cover the range from 3.5 to 30 Å up to now.[2–3] Single-shell tubules are very useful in measuring various physical properties and verifying theoretic predictions.[4–8] A graphene tubule in the absence of a B field was predicted to be a metal or semiconductor.[4–7] In this work, the electronic structure of a chiral tubule threaded by a parallel B field is calculated by the tight-binding model.[6] It is used in studying the magnetic properties, magnetization (M), and differential susceptibility (χ_M) of the single-shell graphene tubule. We mainly study the effects due to the spin-B interaction, the geometric structure, the temperature (T), and the doping.

The band property, metal or semiconductor, of a graphene tubule was predicted to rely on the radius and the chiral structure about the axis.[4–7] The density of states (DOS) are divergent in $1/\sqrt{E}$ form at certain band bottoms (corresponding to energies that are locally minimum or maximum) for all parabolic subbands, except that the DOS of the linear subbands in a metallic tubule are finite there.[6] The characteristic of the DOS will be reflected in the physical properties, e.g., M and χ_M. A graphene tubule with any chiral angle here exists in a uniform B field along the tubular axis. Its electronic structure, as done in a graphite sheet,[11] is calculated by the tight-binding model, but with the periodic boundary condition along the transverse direction. Ajiki and Ando[8] calculated it by the effective-mass approximation, and obtained an electronic structure which is completely independent of the tubular chirality. These two methods predict a similar band property, but give very different electronic structures. A graphene tubule could drastically change from a metal (semiconductor) to a semiconductor (metal) during variation of the magnetic flux (ϕ). The energy dispersion without the spin-B interaction is periodical in ϕ, with a period $\phi_0=(hc/e)$, as a result of the Aharonov-Bohm (AB) effect. If a graphene tubule is a metal at $\phi=\phi_a$, there are only liner subbands at a certain band bottom. The linear subbands at ϕ_a will become parabolic at other ϕ's, i.e., they at least have a divergent DOS except at ϕ_a. Moreover the other subbands at least have a divergent DOS at any flux. This characteristic of the DOS is not affected by the spin-B interaction.

Ajiki and Ando[8] calculated M and χ_M of the zigzag tubule (chiral angle is zero) at $T=0$. The spin-B interaction is neglected in their calculations, hence χ_M shows logarithmic divergencies at ϕ_a's, where the liner subbands of a metallic tubule just touch the Fermi level ($E_F=0$). The spin-B interaction is currently taken into account in calculating M and χ_M. It could destroy the periodicity of the band property (metal or semiconductor), so that a graphene tubule is a metal at a certain magnetic-flux range including ϕ_a. This paramagnetic interaction makes the subband capable of crossing the Fermi level before the parabolic dispersion of the crossing subband becomes linear. The subband crossing thus happens at ϕ_c, where a graphene tubule is metallic, but the DOS of the crossing subband is divergent in $1/\sqrt{E}$ form there. From previous study,[9] magnetic properties are expected to show special structures, cusps in M, and power divergencies in χ_M, at ϕ_c. The electronic structure obtained by the tight-binding model strongly relies on the chirality, and it varies with the flux through the tubule. The special structures of M and χ_M are examined to see whether the chirality dependence is obvious. Further, M and χ_M are calculated at various temperatures (T's) to understand the broadening effects on the special structures. The power divergencies in χ_M will be replaced by the observable peak structures at low temperature. In addition to the broadening effect, the temperature could reduce the magnetization. But a metallic tubule due to the spin-B interaction may exhibit an anomalous variation of M with T.

In addition to the spin-B interaction, the doping effect could lead to special structures in the magnetic properties. This is the intercalation of metallic atoms[10] and molecules into the graphene tubules. The charge carriers are introduced into the graphene tubule by means of intercalation compounds (GIC's),[12] carbon fibers,[13] and doped C_{60}.[14] The metallic atoms K and Rb (Ref. 10) have been successfully intercalated into the graphene tubules. Here the electrons are transferred from the metallic atoms to the carbon atoms. Each carbon atom is assumed to receive $0.1e$ on average as found in X_6C_{60} (Ref. 14) ($X=$K, Rb, and Cs) and stage-1 GIC's (C_8X).[12] The Fermi level (E_F) thus increases from zero to a finite value according to the rigid-band model, which is similar to that employed for GIC's.[15–17] The free carriers in the conduction bands will make a large contribution to the physical properties. The doping is thus expected to affect the physical properties obviously, e.g., phonon modes[7] and magnetization.

When ϕ varies, the free carriers will redistribute themselves among the different conduction bands according to the variations of energy dispersions with ϕ. The Fermi level also varies with ϕ to keep the particle number constant. The electronic redistribution is directly reflected in the magnetic properties, and will result in the special structures, cusps in M and sharp peaks in χ_M, at ϕ_c's, where the Fermi level crosses the bottoms of conduction bands. There are several special structures within ϕ_0 even without the spin-B interaction. Hence it is very different than that in the undoped tubule. Compared with that of an undoped tubule, the magnitude of the magnetic response is obviously increased by the doping. It indicates that the magnetic measurements of the special structures are relatively easy for a doped tubule. The magnitude of the magnetic response hardly depends on the radius of an undoped tubule.[8] This property is examined whether it remains so for the doped tubule. If an undoped tubule is a metal (semiconductor) at $\phi=0$, then the magnetism belongs to paramagnetism (diamagnetism) at the small flux.[8] The magnetism is possibly altered by the doping, because the contribution due to the free carriers in the conduction bands is very important. A detailed study is made of the relation between magnetism and the density of free carriers (or Fermi energy).

Magnetization in a graphene tubule is closely related to the persistent currents observed in rings with mesoscopic radii.[18–20] Magnetization here consists of the persistent currents circulating a graphene tubule and the spin polarization. For a large tubule with radius ~ 100 Å, the former is the main contribution, and the latter is small if $\phi\sim\phi_0$. The persistent currents in mesoscopic rings are easily evaluated from the average of the transverse velocity.[21,22] Although the electronic structure here is very complicated, we are also able to obtain persistent currents in a graphene tubule from the average of the transverse velocity by calculating the gradient of the Hamiltonian.[23] However, a simply linear relation, as found in mesoscopic rings, between the current carried by each state and the angular momentum does not exist in a graphene tubule. The magnetic susceptibility of a graphene tubule is $10-10^3$ times larger than that of a mesoscopic ring.[18–22] Hence the special structures in the magnetic properties, the anomalous temperature effects, and the doping effects should be observable in magnetic measurements.

This paper is organized as follows. The electronic structure of a graphene tubule threaded by a parallel B field is calculated in Sec. II by using the tight-binding model. Both magnetization and differential susceptibility are evaluated in Sec. III. The spin-B interaction is taken into account to study the special features shown in magnetization and differential susceptibility. Effects due to temperature and chirality are also discussed. Further, doping effects on the magnetic properties are given in Sec. IV. Finally, some concluding remarks are made in Sec. V.

II. ELECTRONIC STRUCTURE IN A B FIELD

The electronic structure in the presence of a uniform B field parallel to the tubular axis is simply reviewed. A graphene tubule could be regarded as a rolled-up graphite sheet, as shown in Fig. 1(a). It is formed by rolling the sheet from the origin to the vector

$$\mathbf{R}_x = m\mathbf{a}_1 + n\mathbf{a}_2 , \tag{1}$$

where $\mathbf{a}_1=\sqrt{3}b\mathbf{e}_{x'}$ and $\mathbf{a}_2=(\sqrt{3}/2)b\mathbf{e}_{x'}-\frac{3}{2}b\mathbf{e}_{y'}$. $\mathbf{a}_1$ and $\mathbf{a}_2$ are the primitive lattice vectors of the graphite sheet. $\mathbf{e}_{x'}$ ($\mathbf{e}_{y'}$) is the unit vector along the x' axis (y' axis), and $b=1.42$ Å is the nearest-neighbor distance. Any chiral tubule could be determined by $\mathbf{R}_x$, and so the pair of the parameters (m,n) will be used to represent it. The chiral angle of the (m,n) tubule, $\theta=\tan^{-1}(-\sqrt{3}n)/[(2m+n)]$, is the angle between vector $\mathbf{R}_x(\|\mathbf{e}_x)$ and $\mathbf{e}x'$, and the tubular radius is $r=[b\sqrt{3(m^2+mn+n^2)}]/(2\pi)$. It is sufficient to confine the chiral angle to $|\theta|\leq 30°$ to account for all graphene tubules because of the hexagonal symmetry. Also shown in Fig. 1(a) is the primitive vector $\mathbf{R}_y(\|\mathbf{e}_y)$ along the tubular axis. The rectangle, which is bounded by $\mathbf{R}_x$ and $\mathbf{R}_y$, exemplifies the unity cell of the unrolled $(5,-1)$ tubule with $\theta=10.89°$. The number of carbon atoms in a tubular unit cell is $N_u=4\sqrt{(p^2+pq+q^2)(m^2+mn+n^2)/3}$, since each carbon atom occupies an area $3\sqrt{3}b^2/4$ on an average.

It is convenient to take the coordinate (x,y) in expressing the electronic structure including the B field. The Brillouin zone (hexagon) of the graphite sheet and that (rectangle) of the unrolled tubule with periodical vector $\mathbf{R}_x$ and primitive vector $\mathbf{R}_y$ are plotted in Fig. 1(b). The length and width of that rectangle are $(2\pi)/[b\sqrt{3(m^2+mn+n^2)}]$

and $(2\pi)/[b\sqrt{3(p^2+pq+q^2)}]$, respectively. A chiral tubule further needs to satisfy the periodic boundary condition, and so it only has a 1D Brillouin zone (first) along the segment ΓW, i.e., the axial wave vector confined within the first Brillouin zone is $|k_y| \le (\pi)/[b\sqrt{3(p^2+pq+q^2)}]$. A chiral graphene tubule here is in the presence of a uniform B field parallel to $\mathbf{e}_y$. The gauge $\mathbf{A}=\mathbf{B}\times\mathbf{r}/2(\|\mathbf{e}_x)$, is chosen such that wave vector $\mathbf{k}=-i\nabla+(e/c\hbar)\mathbf{A}$. The periodic boundary condition under such gauge is $\Psi(\mathbf{r}+\mathbf{R}_x)=\Psi(\mathbf{r})$, where $\Psi(\mathbf{r})$ is the Bloch function. The transverse wave vector obtained from this condition is $k_x=(2\pi[J+(\phi/\phi_0)])/[b\sqrt{3(m^2+mn+n^2)}][J=1,2,\ldots,(N_u/2)]$, and the corresponding positive integer J serves as the angular momentum or the subband index (see below).

The electronic structure of the (m,n) tubule is calculated by the tight-binding model, as employed for a graphite sheet,[11] and is given by

$$E(k_x,k_y,\sigma,\phi)=E(k_x,k_y,\phi)+E(\sigma,\phi)\ , \tag{2a}$$

where

$$E(k_x,k_y,\phi)=\pm\gamma_0\left\{1+4\cos\left[\frac{3b}{2}(k_y\cos\theta+k_x\sin\theta)\right]\cos\left[\frac{\sqrt{3}b}{2}(k_y\sin\theta-k_x\cos\theta)\right]\right.$$
$$\left.+4\cos^2\left[\frac{\sqrt{3}b}{2}(k_y\sin\theta-k_x\cos\theta)\right]\right\}^{1/2} \tag{2b}$$

and

$$E(\sigma,\phi)=\frac{g\sigma}{m^*r^2}\frac{\phi}{\phi_0}\ . \tag{2c}$$

The quantity $\gamma_0=3.033$ eV (Ref. 6) is the resonance integral for the nearest-neighbor interaction. The spin-B interaction $E(\sigma)=(g\sigma=m^*r^2)(\phi/\phi_0)$ is important here, because it greatly affects the magnetic properties of a graphene tubule (see Sec. III). The g factor is taken to be the same as that ($\simeq 2$) of the pure graphite or GIC's.[12] $\sigma=\pm\frac{1}{2}$ is the electron spin, and m^* is the bare electron mass.

The electronic structure, as is clear from Eq. (2b), is the same for two graphene tubules with opposite chiral angles ($\pm\theta$) and wave vectors ($\pm k_y$) simultaneously. The form of the energy dispersion is relatively simple for two kinds of graphene tubules: zigzag type ($\theta=0°$) and armchair type ($\theta=\pm30°$).[6] Their respective energy dispersions, without the spin-B interaction, are

$$E(k_x,k_y,\phi)_{\text{zigzag}}$$
$$=\pm\gamma_0\left\{1+4\cos\left[\frac{3bk_y}{2}\right]\cos\left[\frac{\sqrt{3}bk_x}{2}\right]\right.$$
$$\left.+4\cos^2\left[\frac{\sqrt{3}bk_x}{2}\right]\right\}^{1/2} \tag{3a}$$

and

$$E(k_x,k_y,\phi)_{\text{armchair}}$$
$$=\pm\gamma_0\left\{1+4\cos\left[\frac{\sqrt{3}bk_y}{2}\right]\cos\left[\frac{3bk_x}{2}\right]\right.$$
$$\left.+4\cos^2\left[\frac{\sqrt{3}bk_y}{2}\right]\right\}^{1/2}\ , \tag{3b}$$

where both $(\sqrt{3}bk_x/2)_{\text{zigzag}}$ and $(3bk_x/2)_{\text{armchair}}$ are equal to $(\pi/m)[J+(\phi/\phi_0)]$ $(J=1,2,\ldots,2m)$. Armchair tubules are metals (see the following condition) at $\phi=0$.

The band properties at $\phi=0$ are first discussed as follows. They are determined by the $E(k_x,k_y,\phi=0)$ term in Eq. (2b). Valence and conduction bands of a graphite sheet are degenerate at corners[11] of the hexagonal Brillouin zone, e.g., the K point shown in Fig. 1(b). Hence a graphene tubule is suggested to be a 1D metal, when $\mathbf{R}_x\cdot\Gamma K=2\pi\times$integer (periodic boundary condition), i.e., $2m+n=3\times$integer.[6] The other cases belong to the semiconducting tubules. The electronic structure of the metallic tubule with $(m,n)=(5,-1)$ is taken as an example. There are $N_u(=28)$ occupied valence bands (include two spins; $E_F=0$) as seen in Fig. 1(c). The other symmetric conduction bands (not shown) are unoccupied. The energy dispersion of the J subband at $+k_y$ is the same as that of the $(N_u/2)-J$ subband at $-k_y$ (not shown). Each subband here is nondegenerate for different J's, but subbands might be degenerate for a tubule with $\theta=0°$and $\pm30°$ [see Eqs. (3a) and (3b)]. Valence and conduction bands are degenerate and linear relative to the H point for $J=11$ [or $k_x=(22\pi)/b\sqrt{63})$]. For a metallic tubule, the H point is located at $\frac{2}{3}\Gamma W(\Gamma)$ [see Fig. 1(b)], if $n-m$ is equal (unequal) to $3d\times$integer.[7] d is the highest common divisor of m and n. Moreover, the DOS of the only linear subbands relative to the H point are finite, and all parabolic dispersions at certain band bottoms are divergent in $1/\sqrt{E}$ form. The only difference in the feature of the DOS between metallic and semiconducting tubules is that all subbands in the latter must at least have a divergent DOS in $1/\sqrt{E}$ form.[6,23]

The energy dispersion is changed during the variation of the magnetic flux. When the spin-B interaction is neglected, the energy dispersion in Eq. (2b) is periodic in

ϕ, with a period ϕ_0. The tubules with $2m+n=3\times$integer ($\neq 3\times$integer) are metals at $\phi_a=$integer$\times\phi_0$ [(integer$\pm\frac{1}{3}$)ϕ_0] [see Eqs. (2b), (3a), and (3b)], and they are semiconductors at the other ϕ's. The characteristic of the DOS is that the DOS are divergent in $1/\sqrt{E}$ form for all subbands at any flux except that the only linear subbands relative to the H point have a finite DOS at ϕ_a. The spin-B interaction further destroys the periodicity of the band property (metal or semiconductor), but does not affect the characteristic of the DOS. Therefore, a graphene tubule is a metal at a certain magnetic-flux range including ϕ_a, and each subband has a divergent DOS there except for the linear subbands at ϕ_a. This special relation between band property and the DOS will be directly reflected in the magnetic response.

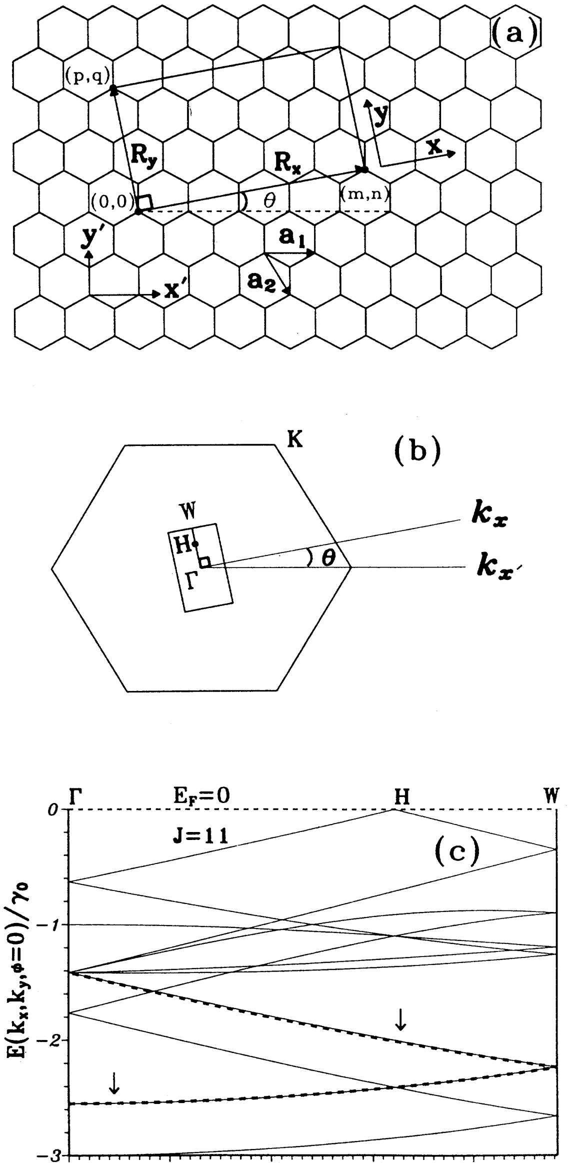

FIG. 1. (a) A graphene tubule is just a graphite sheet rolled from the origin to the vector $\mathbf{R}_x=m\mathbf{a}_1+n\mathbf{a}_2$, where $\mathbf{a}_1$ and $\mathbf{a}_2$ are the primitive vectors of the graphite sheet. The tubular axis is parallel to the primitive vector $\mathbf{R}_y=p\mathbf{a}_1+q\mathbf{a}_2$. The x' and y' axes are relative to the graphite sheet, and the x and y axes are parallel to $\mathbf{R}_x$ and $\mathbf{R}_y$, respectively. That rectangle formed by $\mathbf{R}_x$ and $\mathbf{R}_y$ is the unit cell of the unrolled tubule corresponding to $(m,n)=(5,-1)$. (b) The hexagonal Brillouin zone of the graphite sheet and that (rectangle) of the unrolled tubule. A chiral tubule has the 1D Brillouin zone (first) along the segment ΓW. ΓW here is that of the $(5,-1)$ tubule. The H point is at $\frac{2}{3}\Gamma W$. (c) The energy dispersion of the metallic $(5,-1)$ tubule at $\phi=0$. Each subband is described by the transverse wave vector $k_x(=2\pi J/b\sqrt{63})$ or the angular momentum J. All 28 valence bands are occupied ($E_F=0$), and the symmetric conduction bands are unoccupied (not shown). The arrows point at two subbands close to each other. The valence and conduction bands with $J=11$ are linear and degenerate relative to H point.

III. MAGNETIZATION AND DIFFERENTIAL SUSCEPTIBILITY

The energy dispersion formulated in Eqs. (2a)–(2c) is used in calculating both magnetization and differential susceptibility. The spin-B interaction $(g\sigma/m^*r^2)(\phi/\phi_0)$ included in the energy dispersion is very important, because the 1D subband with the divergent DOS is capable of crossing the Fermi level. M is expected to show special cusps, as indicted from the previous study,[9] as a result of the 1D subband crossings. Furthermore, χ_M exhibits discontinuous divergencies when the subband crossings occur. These features are closely examined, and their chirality dependences are studied. Temperature effects are also included in the study. The results suggest that special structures of the magnetic properties should be measurable at low temperature ($T<1$ K). Moreover, the anomalous variation of M with T exists in a metallic tubule.

The electronic structure varies with the magnetic flux through a tubule. Magnetization at a finite temperature is a variation of the free energy with the magnetic flux. The canonical ensemble (here the same as the grand-canonical ensemble) is taken in evaluating the free energy. The distribution probability of each subband state is described by the Fermi-Dirac function

$$f(E(k_x,k_y,\sigma,\phi)) = \frac{1}{\exp\{\beta[E(k_x,k_y,\sigma,\phi)-\mu(T,\phi)]\}+1}\,, \qquad (4)$$

where $\beta=(k_BT)^{-1}$. The chemical potential $\mu(T,\phi)$ is known to be zero at $T=0$, and remains so at the other T's and ϕ's. The reason why $\mu(T,\phi)=0$ at all T's and ϕ's comes from the symmetric structure of both valence and condition bands; that is, the DOS is symmetric about energy zero. μ here is independent of T and ϕ. However, it does not behave in this way in the doped graphene tubule (see Fig. 12 in Sec. IV). A graphene tubule only exchanges energy with a reservoir, and the particle number is fixed during the flux variation. The free energy per unit length at T is given by

$$F(\phi,T)=\sum_{\sigma,k_x}\int_{1\mathrm{st}}\frac{dk_y}{2\pi}\frac{-1}{\beta}\ln\{1+\exp[-\beta E(k_x,k_y,\sigma,\phi)]\}\ . \tag{5}$$

The integration of dk_y is confined to the first Brillouin zone.

The magnetization at T is calculated from the definition

$$M(\phi,T)=-c\frac{\partial F(\phi,T)}{\partial\phi}\ . \tag{6}$$

The magnetization here includes both the persistent currents circulating in a graphene tubule and the spin polarization. If the spin-B interaction is neglected, the magnetization is equal to the persistent current density (per unit length), and their directions are perpendicular to each other. The persistent current carried by each subband state corresponds to the average of the transverse velocity. This average value could be evaluated from the gradient of the Hamiltonian versus k_x;[23] therefore, we obtain the same persistent currents from such calculation. Substituting Eqs. (2a) and (5) into Eq. (6), $M(\phi,T)$ of the (m,n) tubule is thus given by

$$M(\phi,T)=-c\sum_{\sigma,k_x}\int_{1\mathrm{st}}f(E(k_x,k_y,\sigma,\phi))\left\{\frac{\partial E(k_x,k_y,\phi)}{\partial\phi}+\frac{g\sigma}{m^*r^2\phi_0}\right\}\frac{dk_y}{2\pi}\ , \tag{7a}$$

where

$$\begin{aligned}\frac{\partial E(k_x,k_y,\phi)}{\partial\phi}=\frac{\pm 2\pi\gamma_0^2}{E(k_x,k_y,\phi)\sqrt{m^2+mn+n^2}}\Bigg\{&\cos\theta\sin[\sqrt{3}b(k_y\sin\theta-k_x\cos\theta)]\\ &-\sqrt{3}\sin\theta\sin\left[\frac{3b}{2}(k_y\cos\theta+k_x\sin\theta)\right]\cos\left[\frac{\sqrt{3}b}{2}(k_y\sin\theta-k_x\cos\theta)\right]\\ &+\cos\theta\cos\left[\frac{3b}{2}(k_y\cos\theta+k_x\sin\theta)\right]\sin\left[\frac{\sqrt{3}b}{2}(k_y\sin\theta-k_x\cos\theta)\right]\Bigg\}\ .\end{aligned} \tag{7b}$$

The origination of $M(\phi,T)$, as seen from Eq. (7a), is very complicated. The first term $\partial E(k_x,k_y,\phi)/\partial\phi$ in Eq. (7b), which is related to the persistent current density, consists of both the axial wave vector and the transverse wave vector (or the angular momentum). Consequently, the simply linear relation, as found in a mesoscopic ring,[21,22] between current carried by each state and angular momentum does not exist here. Derivative of $M(\phi,T)$ versus ϕ is the differential susceptibility

$$\chi_M(\phi,T)=\pi r^2\mu_0\frac{\partial M(\phi,T)}{\partial\phi}\ , \tag{8}$$

where $\mu_0(=4\pi\times 10^{-7}\ \mathrm{N/A^2})$ is the free-space magnetic permeability.

The zigzag tubule is the main object of study, since the special features shown in the magnetic response are easily understood from its relatively simple electronic structure [see Eq. (3a)], and there is no loss of generality. The magnetization at $T=0$ is first studied; $M(\phi,T)$ in Eq. (7a) for a zigzag tubule ($\theta=0°$) is thus reduced to

$$M(\phi,T=0)_{\mathrm{zigzag}}=-c\sum_{\sigma,J}^{\mathrm{occu.}}\int_{1\mathrm{st}}\left\{\frac{\dfrac{\mp 2\pi\gamma_0}{m\phi_0}\sin\left[\dfrac{\pi}{m}\left[J+\dfrac{\phi}{\phi_0}\right]\right]\left\{2\cos\left[\dfrac{\pi}{m}\left[J+\dfrac{\phi}{\phi_0}\right]\right]+\cos\left[\dfrac{3bk_y}{2}\right]\right\}}{\left\{1+4\cos\left[\dfrac{3bk_y}{2}\right]\cos\left[\dfrac{\pi}{m}\left[J+\dfrac{ph}{\phi_0}\right]\right]+4\cos^2\left[\dfrac{\pi}{m}\left[J+\dfrac{\phi}{\phi_0}\right]\right]\right\}^{1/2}}+\frac{g\sigma}{m^*r^2\phi_0}\right\}\Bigg|_{E(J,k_y,\sigma,\phi)\le 0}\frac{dk_y}{2\pi}\ . \tag{9}$$

Each occupied subband is limited by the condition $E(k_x,k_y,\sigma,\phi)\leq 0$ because of $E_F=0$. The dk_y integral range close to the subband bottom (corresponding to $k_y=0$ for a zigzag tubule) will depend on the magnetic flux, when the subband with the spin-B interaction intersects with the Fermi level.

(210,0) and (211,0) tubules are calculated for their magnetization and differential susceptibility. The former has a radius $r=82.22$ Å, and the latter $r=82.59$ Å. The B field corresponding to ϕ_0 is 19.47 T (19.29 T) for the former (latter). Respectively, they are metallic and semiconducting (gap ~ 0.05 eV) at $\phi=0$. Each subband represented by J, as seen from Eq. (3a), is double degenerate except that two subbands $J=m$ and $2m$ of the metallic tubule are nondegenerate. The band property will affect the characteristics of magnetization and differential susceptibility. The larger tubules here are chosen for a model study; however, the smaller tubules could also exhibit similar magnetic properties.

$M(\phi,T=0)$ of the (210,0) tubule is shown in Fig. 2. The dashed curve is the result in which the spin-B interaction is neglected. $M(\phi,T=0)$ is a periodic function (period ϕ_0), and it is antisymmetric about $\phi_0/2$. $M(\phi,T=0)$ in Eq. (9) could be simply expressed as

$$\sum_J^{\text{occu.}} \sin\left[\frac{\pi\left[J+\dfrac{\phi}{\phi_0}\right]}{m}\right] f\left[\cos\left[\frac{\pi\left[J+\dfrac{\phi}{\phi_0}\right]}{m}\right]\right] ;$$

therefore, both periodicity and antisymmetry are easily identified from $M(\phi,T=0)=M(\phi+\phi_0,T=0)=-M(\phi_0-\phi,T=0)$. Both periodicity and antisymmetry, as seen in the solid curve, are destroyed by the inclusion of the spin-B interaction. A pair of detailed cusps in the neighborhood of ϕ_0 are shown in the inset, and other pairs occur at the positions close to $2\phi_0, 3\phi_0, \ldots$, etc. $M(\phi,T=0)$ is independent of the spin-B interaction except in the flux regions confined by a pair of cusps. $M(\phi,T=0)$ at $\phi=0$ is vanishing, because the persistent currents coming from the two subbands J and $2m-J$ cancel each other. They do not behave as stated above for a graphene tubule with $\theta\neq 0°$ or $\pm 30°$, but the net magnetization is still vanishing at $\phi=0$. The cancellations remain significant at any ϕ; hence the magnitude of M is small.

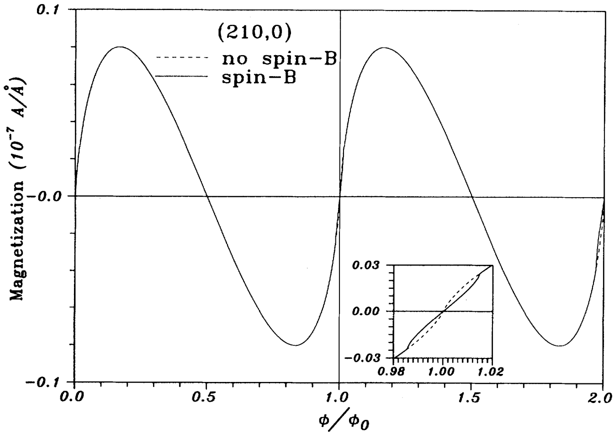

FIG. 2. Magnetization $M(\phi,T=0)$ of the (210,0) tubule. The dashed and solid curves, respectively, are calculated without and with the spin-B interactions. The spin-B interaction destroys the period ϕ_0. The inset shows the details around the cusps at $\phi\sim\phi_0$.

The cusps in $M(\phi,T=0)$ deserve a closer examination. The electronic structure varies as from Eq. (3a) as ϕ changes. The bottoms of the subbands denoted by $J_a=139$ and 279 only touch the Fermi level at $\phi=\phi_0$, when the spin-B interaction is discarded. The DOS of these two linear subbands are finite there, and so there are no cusps in $M(\phi,T=0)$. $M(\phi,T=0)$ behaves the same but there are logarithmic divergencies in $\chi_M(\phi,T=0)$ (Ref. 8) (see the open circles in Fig. 8 at $\phi\sim\phi_0$). Although the spin-B interaction is small for $\phi\sim\phi_0$, it is the main factor in determining the existence of a pair of cusps, as seen in the inset. For example, the spin-B interaction $(g\sigma/m^*r^2)(\phi/\phi_0)\simeq 1.13$ meV at $\phi=\phi_0$. As a result of the spin-B interaction, both $J_a=139$ and 279 subbands just cross the Fermi level at $\phi_c-0.9858$ (1.0145) ϕ_0 for the first (second) cusp. At $\phi=\phi_c$, the DOS of the crossing subbands at the band bottom ($k_y=0$) are further found to be divergent in $1/\sqrt{E}$ form from the calculation of $|dE(J_a,k_y,\phi_c)/dk_y|^{-1}[\propto 1/\sin(3bk_y/2)]$. Consequently, the divergency of the DOS at the band bottom leads to the cusps in $M(\phi,T=0)$. The cusps, as known from a previous study,[9] suggest that the electron populations undergo drastic change there. In addition to the variation of the electronic structure with the flux, the electrons could redistribute themselves between valence (spin-up) and conduction (spin-down) bands with the same J_a. The redistribution only occurs within the magnetic-flux region confined by a pair of cusps. Concerning a pair of cusps, the crossing conduction-band (valence-band) states become occupied (vacant) at the first cusp, and vacant (occupied) at the second cusp. Furthermore, the electron redistribution could cause an anomalous temperature effect (see below). Because subbands with divergent DOS's intersect the Fermi level within a certain magnetic-flux range (see below), the spin-B interaction also has an obvious effect on the transport properties and the thermal properties. This paramagnetic interaction is found to result in special step structures in the ballistic magnetoconductance (the quantized conductance),[24] and divergent structures (in $1/\sqrt{T}$ form) in the heat capacity.[25]

The cusp responds to the fact that the J_a subband bottom crosses the Fermi level, and the crossing position ϕ_c thus satisfies the relation: $[E(J_a,k_y=0),0,\phi_c)_{\text{zigzag}}| = |g\sigma/m^*r^2|$. An approximate ϕ_c could be obtained from expanding $E(J_a,k_y=0,\phi)_{\text{zigzag}}$ in the neighborhood of ϕ_a, where the dispersion of the J_a subband is linear, e.g., $\phi_a=\phi_0$ for a pair of cusps shown in the inset. ϕ_c is approximately given by

$$\phi_c\simeq[1\mp C_1+O(C_1^2)]\phi_a\ , \tag{10}$$

where $C_1=|g\sigma/m^*r^2|/(\sqrt{3}\pi\gamma_0)/(\sqrt{m^2+mn+n^2})$, and it is about 0.014 for the (210,0) tubule. There is no solution for a very small θ_c; that is, no cusp, as observed from Fig. 2, is shown at ϕ close to 0. The $-$ ($+$) in Eq. (10) corresponds to the first (second) cusp of a pair of cusps. The magnetic-flux range ($\simeq 2C_1\phi_a$) in which a pair of cusps exists is approximately proportional to the magnetic flux. It is about $0.029\phi_0$ for ϕ_c near to ϕ_0, as shown in the inset. For a graphene tubule with any chiral angle, the approximate expression of ϕ_c in Eq. (10) remains in similar form.

$M(\phi,T=0)$ of the (211,0) tubule is plotted in Fig. 3. The dashed and solid curves, respectively, correspond to those without and with spin-B interactions. Both periodicity and symmetry in the absence of the spin-B interaction, and the aperiodicity due to this interaction, are similar to those (see Fig. 2) of the (210,0) tubule. The notable differences, as observed from a comparison of the insets here with that shown in Fig. 2, between (211,0) and (210,0) tubules lie in the flux region close to a pair of cusps. There are two pairs of cusps within one ϕ_0 for the (211,0) tubule, but only one pair for the (210,0) tubule. The cusps here occur in the neighborhood of $\phi_a=(\text{integer}\pm\frac{1}{3})\phi_0$ [see Eq. (3a)], where the (211,0) tubule is a metal in the absence of the spin-B interaction. The pair of cusps close to $\frac{2}{3}\phi_0$ ($\frac{1}{3}\phi_0$) comes from the crossing of the $J_a=140$ ($J_a=281$) subband. The approximate crossing position of the (211,0) tubule also satisfies Eq. (15), but the flux range between a pair of cusps is narrower for the smaller ϕ_a (or weaker spin-B interaction). For example, the flux range is about $0.0185\phi_0$ for the second pair of cusps as shown in the upper inset of Fig. 3. Another difference is that the direction of magnetization is opposite between (211,0) and (210,0) tubules. The graphene tubule with $2m+n\neq 3\times\text{integer}(=3\times\text{integer})$ is basically diamagnetic (paramagnetic) at the small flux,[8] e.g., diamagnetism for the (211,0) tubule. These stated differences depend only on the band property, metal or semiconductor, in the absence of the B field. In addition, the magnetism could further be altered by the doping, and is mainly determined by the finite Fermi energy (see Sec. IV).

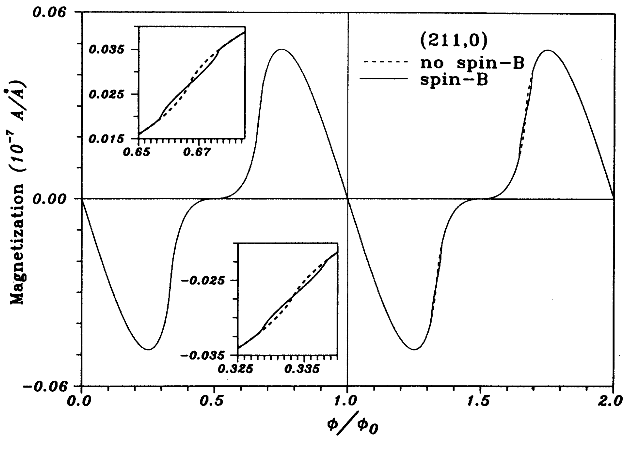

FIG. 3. Same plot as Fig. 2, but for the (211,0) tubule. The upper and lower insets, respectively, show the details around the cusps at $\phi\sim\frac{2}{3}\phi_0$ and $\sim\frac{1}{3}\phi_0$.

The differential susceptibility $\chi_M(\phi,T=0)$, including the spin-B interaction, is shown in Fig. 4. The dashed-dotted and dashed-circled curves correspond to the (210,0) and (211,0) tubules, respectively. The order of χ_M is 10^{-4}–10^{-5}. Two kinds of divergent forms, logarithmic and power forms, are found at the positions near $\phi=0$ and $\phi=\phi_c$, respectively. The logarithmic divergency shown in the dotted-dashed curve occurs at $\phi=0$, where there is no subband crossing. It also exhibits at $\phi=\phi_a$ (e.g., open circles in Fig. 8), when the spin-B interaction is neglected.[8] The logarithmic divergency reflects the fact that the linear valence and conduction bands just touch the Fermi level. It is related to the $J_a=140$ and 280 subbands of the (210,0) tubule. This logarithmic divergency at $\phi=0$ could be understood from the derivative of the definite integral in Eq. (9):

$$\frac{\partial M(\phi,T=0)_{\text{zigzag}}}{\partial\phi}\propto\frac{\partial}{\partial\phi}\int_{k_{y,-}(\phi)}^{k_{y,+}(\phi)}f(k_y,\phi)dk_y$$

$$\propto\int_{k_{y,-}(\phi)}^{k_{y,+}(\phi)}\frac{\partial f(k_y,\phi)}{\partial\phi}dk_y+\frac{\partial k_{y,+}(\phi)}{\partial\phi}f(k_{y,+}(\phi),\phi)=\frac{\partial k_{y,-}(\phi)}{\partial\phi}f(k_{y,-}(\phi),\phi)\ , \tag{11a}$$

where

$$f(k_y,\phi)=\frac{-c}{\pi\phi_0}\sum_{\sigma,J_a}\left\{\frac{\dfrac{\mp 2\pi\gamma_0}{m}\sin\left[\dfrac{\pi}{m}\left[J_a+\dfrac{\phi}{\phi_0}\right]\right]\left\{2\cos\left[\dfrac{\pi}{m}\left[J_a+\dfrac{\phi}{\phi_0}\right]\right]+\cos\left[\dfrac{3bk_y}{2}\right]\right\}}{\left[1+4\cos\left[\dfrac{3bk_y}{2}\right]\cos\left[\dfrac{\pi}{m}\left[J_a+\dfrac{\phi}{\phi_0}\right]\right]+4\cos^2\left[\dfrac{\pi}{m}\left[J_a+\dfrac{\phi}{\phi_0}\right]\right]\right]^{1/2}}+\frac{g\sigma}{m^*r^2}\right\}\ . \tag{11b}$$

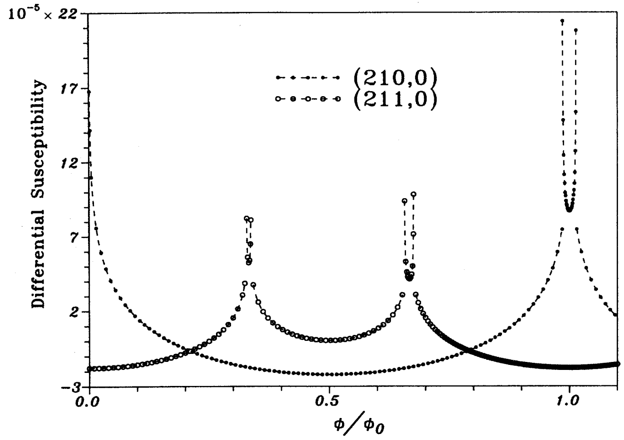

FIG. 4. The differential susceptibility $\chi_M(\phi,T=0)$, including the spin-B interaction. The dashed-dotted and dashed-circled curves, respectively, are those of the (210,0) and (211,0) tubules.

The above equations are valid for any flux, and it is sufficient in considering the divergent forms that subbands in the summation $\sum_{\sigma,J_a}$ are only for those touching or crossing the Fermi level. The integral upper limit $k_{y,+}(\phi)$ is the axial wave vector corresponding to the lowest (highest) energy of the occupied valence (condition) band, and the integral lower limit $k_{y,-}(\phi)$ is the opposite. At $\phi\sim 0$, the integral limits are independent of ϕ there because of no subband crossing, i.e., $k_{y,-}=0$ and $k_{y,+}=(\pi/3b)$ stay the same for the zigzag tubule. Therefore, they do not contribute to the derivative of M versus ϕ, and $\partial f(k_y,\phi)/\partial\phi$ in Eq. (11a) is the only contribution of the logarithmic divergency. When $f(k_y,\phi)$ in Eq. (11b) is expanded about the small ϕ and k_y for the $J_a=140$ and 280 subbands, its derivative versus ϕ is approximately given by $(k_y^2+3(\pi\phi/m)^2)^{-1/2}$. $\chi_M(\phi,T=0)$ is then proportional to $-\ln|\phi|$ by substituting the above approximation into the first term in Eq. (11a).

Each power divergency shown in the two curves is located at ϕ_c, where the J_a subband just crossed the Fermi level. The divergency at $\phi_c=0.9858\phi_0$ in the dashed-dotted curve (also see the solid circles in Figs. 6 and 8) is taken as an example to realize the general power form. It is related to the $J_a=139$ and 279 subbands of the (210,0) tubule. The finite $\chi_M(\phi,T=0)$ at the left-hand neighborhood ($\phi_{c,-}$) only reflects the fact that no subband crossing occurs there. The divergency at the right-hand neighborhood ($\phi_{c,+}$) results from the variation of the integral limits with ϕ, because the contribution due to the integration of $\partial f(k_y,\phi)/\partial\phi$ in Eq. (11a) is finite. That $\partial f(k_y,\phi_c)/\partial\phi$ is a well-behaved function within the integral range is the main reason. It is noticed that $\partial f(k_y,\phi)/\partial\phi$ remains so even at $\phi=\phi_0$, since the divergency, as found at $\phi=0$, is canceled by the valence and conduction bands. This feature of $\partial f(k_y,\phi)/\partial\phi$ could explain why χ_M here does not show a logarithmic divergency at $\phi=\phi_0$. The integral lower (upper) limit of the occupied conduction (valence) band at $\phi_{c,+}$ is independent of flux; hence the power divergency is related to the derivative of the integral upper (lower) limit versus flux for the occupied conduction (valence) band. The relation between the integral limit and the flux is approximated to be

$$k_{y,\pm}(\phi)\simeq\frac{2}{3b}\left[\left[\frac{g\sigma\phi}{m^*r^2\gamma_0}\right]^2-3\left[\frac{\pi(\phi-\phi_a)}{m}\right]^2\right]^{1/2}$$

[+ (−) is for the occupied conduction (valence) band; $\otimes|\phi-\phi_c|^{1/2}$], when the energy dispersion $|E(J_a,k_y,\phi)_{\text{zigzag}}|-|g\sigma/m^*r^2|$ is expanded about the neighborhood of $k_y=0$ and $\phi=\phi_a$. As a result the term, $[\partial k_{y,+}(\phi)](\partial\phi)f(k_{y,+}(\phi))-[\partial k_{y,-}(\phi)]/(\partial\phi)f(k_{y,-}(\phi))$ in Eq. (11a) makes an outstanding contribution to χ_M in the $|\phi-\phi_c|^{-1/2}$ divergent form. The other power divergencies could similarly be proved to have the same divergent form.

The chirality of a graphene tubule is presently investigated as to whether it strongly affects magnetization and differential susceptibility. Three metallic tubules (at $\phi=0$)—(242,−121), (230,−46), and (210,0)—with the nearly same radii are chosen to show the chiral effect. The corresponding chiral angles and radii are (30°, 10.89°, 0°) and (82.04,82.52,82.22) (Å). The 1D Brillouin zone of the (230,−46) tubule is the same as that [Fig. 1(b)] of the (5,−1) tubule, so these two tubules have similar electronic structures [see Fig. 1(c)]. The magnetization is independent of the opposite chiral angles ($\pm\theta°$), as examined from Eqs. (7a) and (7b) by changing (θ,k_y) to $(-\theta,-k_y)$. $M(\phi,T=0)$ in Eq. (7a) for an armchair tubule [here a (242,−121) tubule] could be further reduced to

$$M(\phi,T=0)_{\text{armchair}}$$

$$=-c\sum_{\sigma,J}^{\text{occu.}}\int_{\text{1st}}\left\{\frac{\dfrac{\mp 2\pi\gamma_0}{m\phi_0}\sin\left[\dfrac{\pi}{m}\left[J+\dfrac{\phi}{\phi_0}\right]\right]\cos\left[\dfrac{\sqrt{3}bk_y}{2}\right]}{\left\{1+4\cos\left[\dfrac{\sqrt{3}bk_y}{2}\right]\cos\left[\dfrac{\pi}{m}\left[J+\dfrac{\phi}{\phi_0}\right]\right]+4\cos^2\left[\dfrac{\sqrt{3}bk_y}{2}\right]\right\}^{1/2}}+\frac{g\sigma}{m^*r^2\phi_0}\right\}$$

$$\times|E(J,k_y,\sigma,\phi)\le 0\frac{dk_y}{2\pi}\ . \tag{12}$$

The interesting flux range is that close to the subband crossing or $\phi=\phi_0$. Magnetization and differential susceptibility in that region, respectively, are shown in Figs. 5 and 6. The results, as observed from those in Figs. 5 and 6, are very close to one another, although there are many differences in the electronic structures among three tubules, e.g., the subband degeneracies. The features like cusps in $M(\phi,T=0)$ and power divergencies in $\chi_M(\phi,T=0)$, are related to the subband crossings and hence hardly depend on the chirality. Take the (230,−46) tubule as an example. The cusp in M is only related to the $J_a=505$ crossing subband, and its position ϕ_c is approximately obtained by expanding the dispersion $|E(J_a,k_y=\frac{2}{3}\Gamma W,\phi)$ in the neighborhood of ϕ_0. ϕ_c also satisfies the approximate Eq. (10) as does the (210,0) tubule. The power divergency $\propto|\phi-\phi_c|^{-1/2}$ in χ_M is further obtained by expanding the above dispersion at the neighborhood of $k_y=\frac{2}{3}\Gamma W$ [or ΓH in Fig. 1(b)] and $\phi=\phi_0$. Another (242,−121) tubule does behave so. These expansions explain why the essential features shown in M and χ_M are insensitive to the chirality. The chirality only has very weak effect on the magnitude of M and χ_M, as obtained from the results of the metallic and semiconducting (not shown) tubules.

Cusps in M and power divergencies in χ_M at $T=0$ are expected to be broadened by the finite temperature. $M(\phi,T)$ of the (210,0) tubule is shown in Fig. 7 at various temperatures. The results (the shortest-dashed curve) without the spin-B interaction at $T=0$ is also shown for the comparison. The cusps (solid curve) are hardly affected by the temperature at $T\leq 0.1$ K (not shown). They are gradually flattened by the increasing temperatures, and disappear at $T\geq 10$ K. The corresponding $\chi_M(\phi,T)$ is shown in Fig. 8. The power divergencies (solid circles) at $T=0$ are replaced by the peak structures at finite T. If $T>10$ K, the spin-B interaction effects are completely buried by the thermal broadening. This is because the magnitude of the spin-B interaction ($\simeq 1$ meV) corresponds to the thermal energy at $T=10$ K. The broadening effects in the semiconducting (211,0) tubule (not shown) are similar to those shown here. The magnitude of χ_M is about $10-10^2$ times larger than that measured from the mesoscopic rings.[18–22] The peak structures in $\chi_M(\phi,T)$ should be experimentally observable if T is below 1 K.

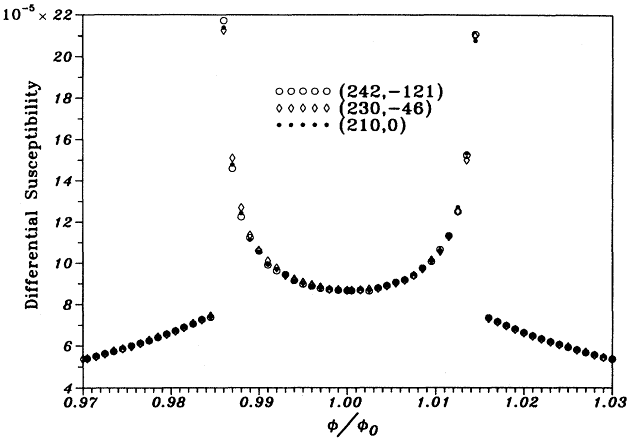

FIG. 6. The differential susceptibility comes from the magnetization shown in Fig. 5.

The temperature does not destroy the period of the AB oscillation as the spin-B interaction does. But it has another important effect in that the magnitude of the magnetization decreases as T increases.[22] That the additional persistent currents due to conduction-band states (vacant states at $T=0$) could reduce the net contribution of the valence-band states is the main reason. It is noted that the variation of spin polarization with temperature is negligible except at the relatively high T. The amplitude of $M(\phi,T=0)$ is situated at $\phi\sim\phi_{/6}$ ($\sim\phi_0/4$) for the tu-

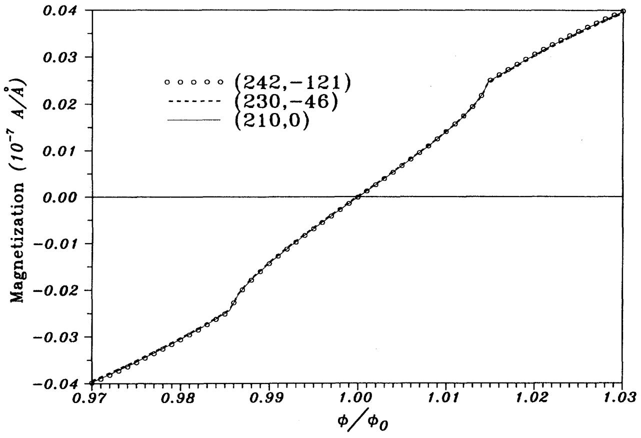

FIG. 5. Magnetization $M(\phi,T=0)$ of the three metallic tubules at the flux close to ϕ_0. They are represented by (242,−121), (230,−46), and (210,0), and their chiral angles are 30°, 10.89°, and 0°, respectively. The results are close to one another.

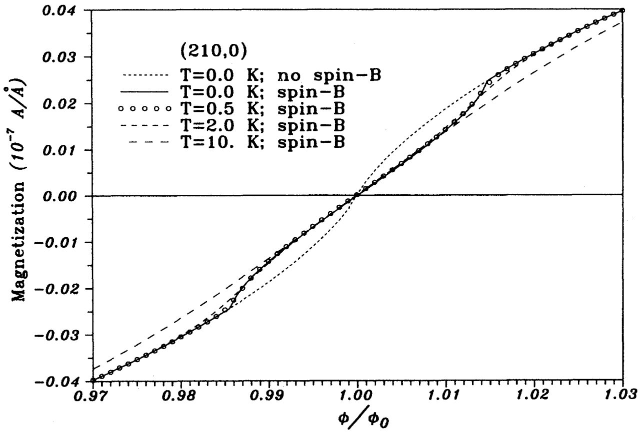

FIG. 7. Magnetization $m(\phi,T)$ of the (210,0) tubule is shown at various temperatures. They include the spin-B interaction, and that (the shortest-dashed curve) without the spin-B interaction at $T=0$ is also shown for the comparison.

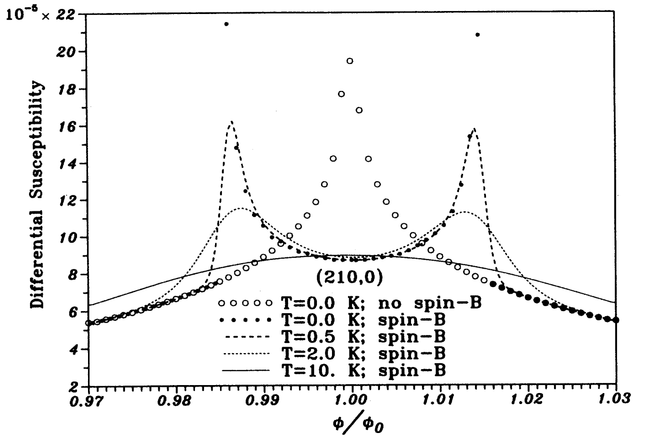

FIG. 8. The differential susceptibility comes from the magnetization shown in Fig. 7.

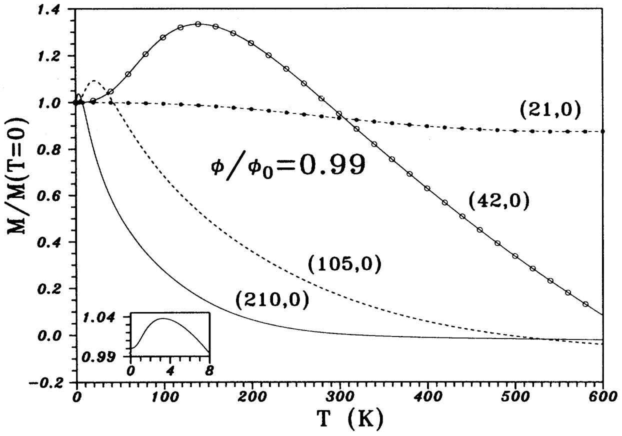

FIG. 10. Same plot as Fig. 9, but shown at $\phi=0.99\phi_0$. The inset shows the details of the (210,0) tubule at low temperature.

bules with $2m+n=3\times$integer ($\neq 3\times$ integer), e.g., the (210,0) [(211,0)] tubule shown in Fig. 2. The variation of M with temperature is shown in Fig. 9 at $\phi=\phi_0/6$ for the various tubules with $2m+n=3\times$ integer. These zigzag tubules are semiconducting at $\phi=\phi_0/6$. They have energy gaps[4] proportional to $1/r$ (somewhat affected by the spin-B interaction), and the largest tubule, the (210,0) tubule, has an energy gap corresponding to ~300 K. With increasing temperature, the occupation probability of electrons in the conduction bands increases. At room temperature, conduction and valence bands that are strongly affected by temperature are only those closest to the Fermi level $E_F=0$. For example, for the (210,0) tubule, these subbands are $J=140$ and 280. A larger tubule has a smaller energy gap and subband energy spacing, so that the cancellation of the persistent currents between conduction and valence bands with the same J is more significant at a fixed temperature. Hence the temperature effect, as seen from Fig. 9, in reducing magnetization is relatively obvious for the larger tubules. The temperature that reduces the amplitude of magnetization at $T=0$ to half of the value is approximately proportional to $1/r$ for the various tubules, as indicated from the energy gaps. It is ~120 K for the (210,0) tubule. This feature is almost independent of the chirality, because the energy dispersions of the subbands closest to the Fermi level behave similarly. Moreover, it stays the same for another kind of tubule with $2m+n\neq 3\times$ integer. The temperature effects mentioned above are shown at the magnetic flux, where a graphene tubule is semiconducting.

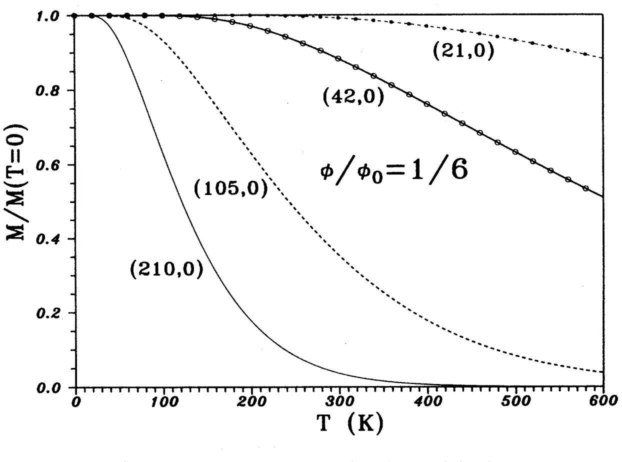

FIG. 9. The variation of magnetization with the temperature is shown at $\phi=\phi_0/6$ for the various zigzag tubules with $2m+n=3\times$integer.

When a graphene tubule is metallic at a certain magnetic-flux range confined by ϕ_c in Eq. (10), the variation of magnetization with temperature may exhibit anomalous behavior. The persistent currents (or M) increase at the relatively low temperature as T increases. Due to the spin-B interaction, the valence J_a subbands intersecting with the Fermi level have vacant states near the band bottom. Hence electrons could occupy those states at $T\neq 0$, and they make a contribution similar to the net contribution of the other valence-band states. When this contribution (increasing persistent currents) is larger than that (decreasing persistent currents) coming from the conduction bands, it causes the anomalous behavior. Figure 10, shown at $\phi=0.99\phi_0$, clearly illustrates such behavior, e.g., the existence of the peak structure. The anomalous behavior also exists in the (21,0) tubule, although there is not a peak structure in the dashed-circled curve. The reason is that the spin polarization (positive) here is larger than the persistent current density (negative), and the main variation of M with T comes from the latter. In addition, the spin polarization might cause the magnetization to change direction and increase with increasing T at relatively high temperature, e.g., M of the (210,0) tubule at $T\sim 500$ K (see the solid curve).

IV. DOPING EFFECT

Graphene tubules could be intercalated with alkali-metal atoms,[10] as was done for doped C_{60} (Ref. 14) and

GIC's.[12] Electrons are transferred from alkali-metal atoms to carbon atoms, and each carbon atom in the saturation composition, as found in X_6C_{60} and stage-1 C_8X, is assumed to receive 0.1 e on an average. Doped zigzag tubules are chosen here for a model study, and the doped armchair tubules are also included to understand the chirality effect. Equation (7a) is used to calculate the magnetization at $T=0$, but the Fermi energy (the chemical potential at $T=0$) in the Fermi-Dirac function needs to vary with ϕ. Owing to the crossings of 1D conduction bands by the Fermi energy, M and χ_M, respectively, are expected to show special cusps and discontinuously sharp peaks. They are calculated for the doped tubules with various radii to see whether the magnetic response markedly relies on the radius. Moreover, M at a small flux is investigated to show the relation between magnetism and Fermi energy [$E_F(\phi=0)$, or free-carrier density].

The electronic structure of the graphene tubule is supposed to remain intact during the intercalation, as employed in the stage-1 GIC's,[15–17] i.e., the effect of the intercalation is restricted to the fixing of the Fermi energy. According to the rigid-band model, the Fermi energy [$E_F(0)$] in the absence of the B field is determined by the free-carrier number per unit length. The relation between the Fermi energy and the linear density could further be obtained from $E(J,k_y,\phi=0)$ in Eq. (2b). The result of the (210,0) tubule is shown in Fig. 11. The cusps (marked by arrows) come from the crossings of the subband bottoms by $E_F(0)$, and they are related to the divergent DOS at the band bottom ($k_y=0$). The linear density of the $(m,0)$ tubule is $D=(0.4m/3b)\ e/\text{Å}$, when each carbon atom is assumed to averagely receive 0.1 e from the intercalant atoms. The assumed linear density of the (210,0) tubule is $D=19.7178\ e/\text{Å}$, and the corresponding energy, as indicated by the solid circle in the inset, is $E_F(0)=2.1311$ eV. The angular momenta corresponding to the occupied conduction bands are within the range $115\le J\le 305$, and the nearest subbands from the Fermi level are $J=305$ and 115. The magnetism at the small flux is principally dependent on D or $E_F(0)$ (see Fig. 18).

A doped graphene tubule only exchanges energy with the reservoir when it exists in a B field. The noninteracting electrons occupy the subbands according to the energy dispersion in Eq. (2a), and the Fermi energy [$E_F(\phi)$] at $T=0$ varies with ϕ to keep the carrier number constant. This behavior is apparently different from that of the undoped tubule, since the Fermi energy always stays the same ($E_F=0$) for the latter (see Sec. III). $E_F(\phi)$ of the (210,0) tubule is shown in Fig. 12. Without the spin-B interaction (dashed curve), $E_F(\phi)$ is periodic in ϕ_0 and symmetric about $\phi_0/2$. Both periodicity and symmetry are easily identified from $E(J,k_y,\phi)=E(J-1,k_y,\phi+\phi_0)$ and $E(J,k_y,\phi)=E(-J-1,k_y,\phi_0-\phi)$. There are four cusps within ϕ_0. The number of cusps depends only on the intrinsic electronic structure. There are four subband bottoms for which energy ranges at $0\le\phi\le\phi_0$ cover $E_F(0)$. This explains why there are four cusps within ϕ_0. The spin-B interaction $E(\sigma,\phi)$, as seen in the solid curve, trivially destroys symmetry and periodicity. The number of cusps is doubled due to the Zeeman splitting for the two spins. Both radius and chirality (not shown) affect only the positions and the number of the cusps, and the essential features shown here remain similar for other doped graphene tubules.

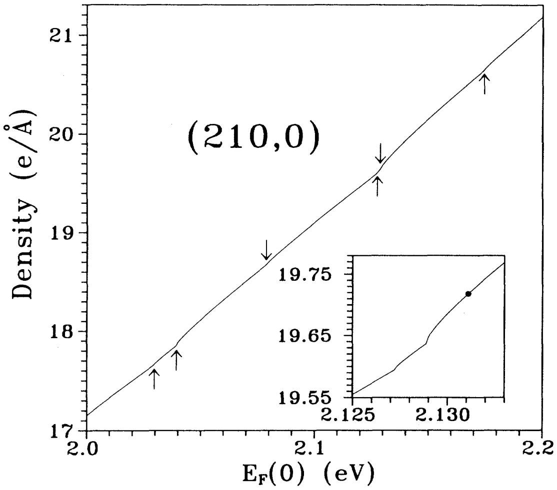

FIG. 11. The relation between the Fermi energy [$E_F(0)$] and the linear free-carrier density (D) is plotted for the (210,0) tubule. The arrows mark the positions of the cusps. The inset shows the details around the assumed density $D=19.7178e/\text{Å}$, which is indicted by the solid circle with $E_F(0)=2.1311$ eV.

The cusps, as stated in Sec. III, imply that the electronic structure undergoes drastic change. However, the electrons here redistribute themselves among the different conduction bands as ϕ varies. The Fermi level $E_F(\phi)$ just crosses the bottom of the J_a conduction band at a certain ϕ_c. The divergency of the DOS at the band bottom thus results in a cusp there. The magnetic property, magneti-

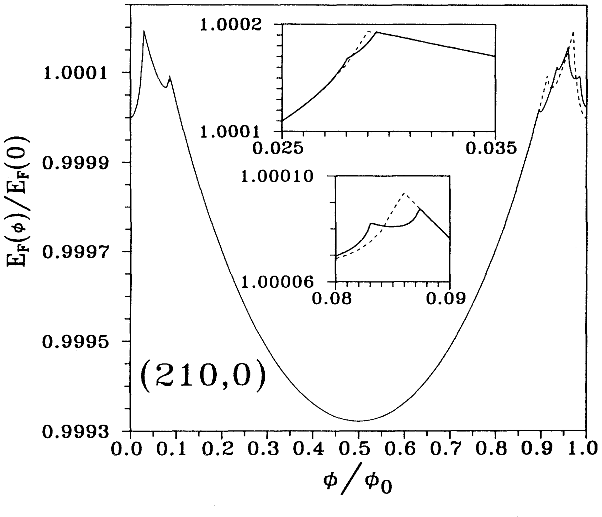

FIG. 12. The variation of the Fermi energy with the magnetic flux is plotted for the (210,0) tubule. The solid and dashed curves, respectively, correspond to those with and without spin-B interactions. The insets show the details around the cusps at the small flux.

zation (see below), is sensitive to the electron distributions; therefore it also exhibits similar cusps. A closer analysis near the cusps could reveal valuable one-body properties (e.g., γ_0 and J), because they are shaped by the one-body electronic structure. The first cusp in the dashed curve (see the upper inset; $\phi_c = 0.029\phi_0$) is taken as an example. It is due to the crossing of the $J_a = 305$ conduction band by $E_F(\phi)$. If ϕ is greater (smaller) than $0.029\phi_0$, the $J_a = 305$ subband is an empty (occupied) subband. The left-hand slope of the cusp could be obtained from the conservation of the free-carrier number,[9] and it is given by

$$\frac{\partial E_F(\phi)}{\partial\phi_{|\phi=\phi_c}} = \frac{\partial E(J_a, k=0, \phi)}{\partial\phi_{|\phi=\phi_c}} = \frac{-2\pi\gamma_0^2 \sin\left[\frac{\pi\left(J_a \frac{\phi_c}{\phi_0}\right)}{m}\right]\left[1+2\cos\left[\frac{\pi\left(J_a+\frac{\phi_c}{\phi_0}\right)}{m}\right]\right]}{m\phi_0 E_F(\phi_c)} . \tag{13}$$

Equation (13) means that the main change of the free-carrier number at ϕ_c comes from the J_a conduction band with the divergent DOS. This exact relation has been checked numerically. Equation (13) remains the similar form for other cusps in the absence of the spin-B interaction, and it only needs to add a Zeeman term, $g\sigma/m^* r^2\phi_0$, for those in the presence of the spin-B interaction. It is useful in understanding the one-body properties of the graphene tubule. The formula of the right-hand slope of the cusp is very complicated, and neglected here. In short, the slope in Eq. (13) is exact at the left-hand (right-hand) neighborhood of the cusp, if the J_a conduction band becomes an empty (occupied) subband at $\phi > \phi_c$ ($\phi < \phi_c$).

We use Eq. (7a) to calculate the magnetization of the doped tubule at $T=0$. $M(\phi)$ of the (210,0) tubule is shown in Fig. 13. The dashed curve is the result in which the spin-B interaction is neglected. $M(\phi, T=0)$ is a periodic function, and is antisymmetric about $\phi_0/2$. Both periodicity and antisymmetry are similar to those in the undoped tubule (see Fig. 2). There are four cusps within ϕ_0 here, but no cusps for the undoped tubule. The reason in explaining the occurrence and number of the cusps is the same as that stated in $E_F(\phi)$. The difference between the doped and undoped tubules arises from the fact that the π-band electrons in the former could redistribute themselves among the different conduction bands, and those in the latter always occupy the same valence bands.

When the spin-B interaction is included, it obviously destroys periodicity and symmetry, as seen in the solid curve. Hence this paramagnetic interaction plays an important role for the doped tubules as well as for the undoped tubule. The result (solid-dotted curve) for the undoped tubule is also shown for comparison. The main differences between the doped and undoped tubules include the number and positions of the cusps, and the magnitude of magnetization. There are eight cusps, as shown in the solid curve, within ϕ_0 for the doped tubule, but only a pair of cusps (at $0.9858\phi_0$ and $1.0145\phi_0$) occur at the neighborhood of ϕ_0 for the undoped tubule. The Zeeman splitting in the doped tubule results in two neighboring cusps coming from the spin-up and -down states, respectively. This behavior is very different from that of the undoped tubule, since a pair of cusps in the latter result from the same spin state. The cusps of the doped tubule possibly occur at a very small flux. For example, the first cusp in the solid curve is at $\phi_c = 0.028\phi_0$ ($B = 0.54$ T; see the upper inset). This implies that the special structures of the magnetization are more easily observed in the doped tubule, owing to the smaller B field. The number and the positions of the cusps basically depend on band dispersion and $E_F(0)$ (or free-carrier density).

Doping could increase the magnitude of the magneti-

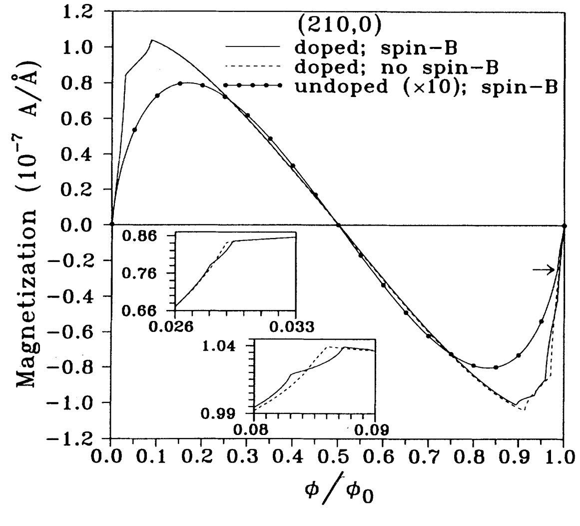

FIG. 13. Magnetization of the (210,0) tubule. The solid and dashed curves, respectively, correspond to those with and without spin-B interactions. The result of the undoped tubule (solid-dotted curve) is also shown for the comparison. The arrow marks the position of the cusp in the undoped tubule. The insets show the details around the cusps at the small flux.

zation by one order. For the doped tubule, the contribution due to all the valence bands is thus inferred to be much smaller than that due to the occupied conduction bands by one order. As a result of the cancellation between the two degenerate subbands $2m-J$ and J, the magnetization is zero at $\phi=0$. Each valence band remains occupied during the variation of the magnetic flux, and, furthermore, the large cancellation similar to the $\phi=0$ case leads to a smaller contribution. However, the contribution due to the two degenerate conduction bands (occupied or unoccupied) nearest to the Fermi level is very important. The reason is that one of the two bands will become unoccupied (or occupied) at $\phi \geq \phi_c$, and the cancellation of the magnetization between them may vanish quickly. Take the magnetization close to the first cusp (see the solid curve in the upper inset) as an example. The Fermi level crosses the bottom of the $J_a=305$ conduction band with spin-up states at $\phi_c=0.028\phi_0$, and this band becomes unoccupied at $\phi>\phi_c$. The magnetization at $\phi=0$ just cancels out for both $J=115$ (positive) and 305 (negative) subbands. Furthermore, the cancellation between them disappears rapidly as the magnetic flux increases gradually. Therefore, the net contribution (positive) due to the $J=115$ and 305 subbands could be regarded as the main contribution of the magnetization at small flux.

$\chi_M(\phi)$, including the spin-B interaction, is shown in Fig. 14. The open circles and the dashed-dotted curve, respectively, correspond to the doped and undoped tubules. χ_M of the undoped tubule exhibits the logarithmic divergency at $\phi \sim 0$ and the power divergency $(1/\sqrt{\phi-\phi_c})$ at $\phi \sim 0.9858\phi_0$, and that of the doped tubule exhibits the discontinuously sharp peaks (divergent) at certain crossing positions. These sharp peaks are related to the derivative of the integral upper limit (or the Fermi momentum) in Eq. (11a) versus ϕ. The approximate Fermi momentum of the J_a conduction band could be obtained from the expansion of the energy dispersion $[E(J_a,k_y,\sigma,\phi)]$ in Eq. (2a) about $k_y=0$ and $\phi=\phi_c$. The derivative of the Fermi momentum versus ϕ is further found to be proportional to $[\partial^2 E_F(\phi)/\partial^2\phi]^{1/2}$. The sharp peaks in χ_M are consistent with the variation of $E_F(\phi)$ with ϕ (see Fig. 2). At low temperatures, these sharp peaks are replaced by the peak structures, as seen in Fig. 6. The magnitude χ_M of the doped tubule is 10^{-3}–10^{-4}, and is about ten times larger than that of the undoped tubule. Furthermore, it is much larger (10^2–10^3 times) than that obtained from mesoscopic metal rings.[18–22] Hence it is relatively easy to observe special structures, cusps in M, and sharp peaks in χ_M in the doped tubule.

For the undoped tubules with $2m+n=3\times$integer ($\neq 3\times$integer), the magnitude of the magnetic response hardly depends on the radius (or m is proportional to $1/r^2$; not shown), and they are paramagnetic (diamagnetic) at the small flux.[8] The doping would have an obvious effect on the above features. The magnetization plotted in Fig. 15 is shown for the various doped tubules with $(m,n)=(210,0)$, (105.0), (42,0), and (21,0). The spin-B interaction is neglected here for simplicity. The carrier number per area is the same for each tubule, and

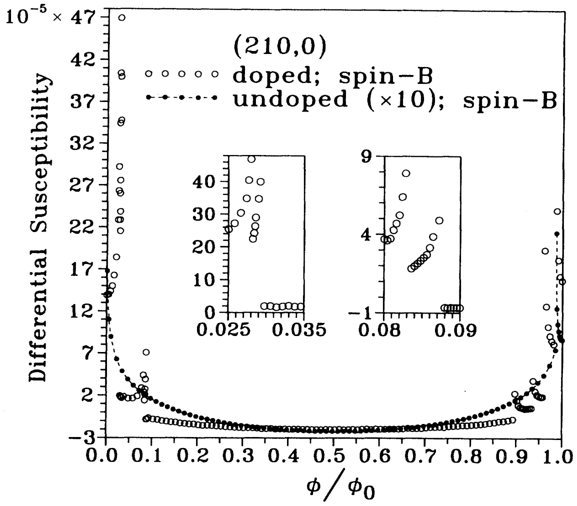

FIG. 14. The differential susceptibility of the (210,0) tubule. The open circles and the dashed-dotted curve, respectively, are those of the doped and undoped tubules in the presence of the spin-B interaction. The insets show the details around the discontinuously sharp peaks (open circles) at the small flux.

the Fermi energy $E_F(0)$ is very close between tubules. The positions of the cusps vary from one tubule to another because of the different electronic structures. If the energy difference $E_D=E_F(0)-E(J_a,k_y=0,\phi=0)$ between $E_F(0)$ and the bottom of the highest (or lowest unoccupied) occupied band is small, then the first cusp shown in $M(\phi)$ would occur at the small ϕ_c. For example, E_D, the (210,0) tubule, is 0.003 eV, and the first cusp is at $\phi_c=0.029\phi_0$. $M(\phi)$ basically shows three kinds of behavior (the third kind shown in Fig. 17). The first kind is that $M(\phi)$ quickly increases at the small flux and then shows a cusp, e.g., $M(\phi)$ of the (210,0) and (42,0) tubules. We could ascribe this behavior to the net contribution of the two degenerate bands $2m-J_a$ and J_a, one of which is crossed by the Fermi level and becomes unoccupied at $\phi>\phi_c$ (as explained in the previous paragraph). The two doped tubules exhibit paramagnetism at small flux, as seen in the undoped case. The second kind of behavior is that $M(\phi)$ of the (105,0) and (21,0) tubules decreases gradually, and the first cusp occurs at the moderate ϕ [e.g., $\phi_c=0.34\phi_0$ for the (21,0) tubule]. These two doped tubules exhibit diamagnetism at small flux. This means that the doping could change the magnetism of the graphene tubule. $M(\phi)$, due to the valence bands, is positive for the undoped tubule with $2m+n=3\times$integer,[8] so that the diamagnetism is related to the contribution of the occupied conduction bands. The linear degenerate conduction bands $J=\frac{2}{3}m$ and $\frac{4}{3}m$ at $\phi=0$ are found to be the main contribution of the diamagnetism. The magnetism of a doped tubule is determined by the competition of the two sets of degenerate bands above. There is not a simple relation between magnetism and radius, as obtained from the calculations, but it is closely related to the Fermi energy (see Fig. 18). The doped graphene tubule may be paramagnetic or diamagnetic, and so are the related GICs.[12,26] The corresponding $\chi_M(\phi)$ is shown in

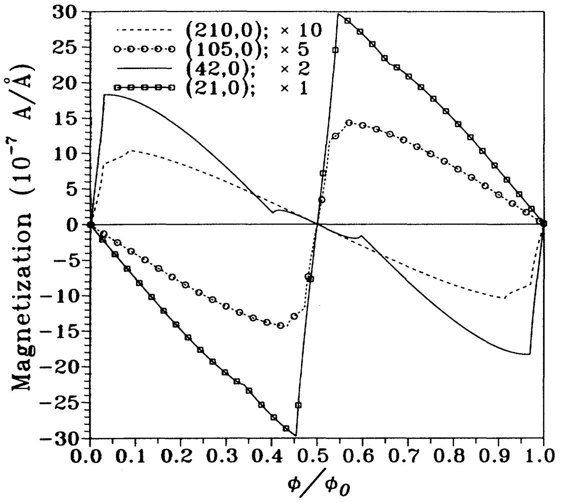

FIG. 15. Magnetization without the spin-B interaction is shown for the various doped tubules with $(m,n)=(210,0)$, (105.0), (42,0), and (21,0).

Fig. 16. The larger the radius, the stronger the magnetic response. Hence, the larger tubules are more suitable in observing the special structures, cusps in M and sharp peaks in $\chi_M(\phi)$. The magnetic response of the doped tubule strongly depends on the radius, but that of the undoped tubule exhibits the opposite feature.[8]

We further study the chirality effect on the magnetization of the doped tubule. $M(\phi)$'s (without spin-B interaction) for the various armchair tubules with $(mn)=(242,-121)$, $(120,-60)$, $(48,-24)$, and $(24,-12)$ are shown in Fig. 17. These armchair tubules, respectively, have nearly the same radii as those of the zigzag tubules shown in Fig. 15. Compared with that of the doped zigzag tubule, the magnetization here is smaller in magnitude, and shows only two cusps within ϕ_0. The differences are mainly caused by the different electronic structures.

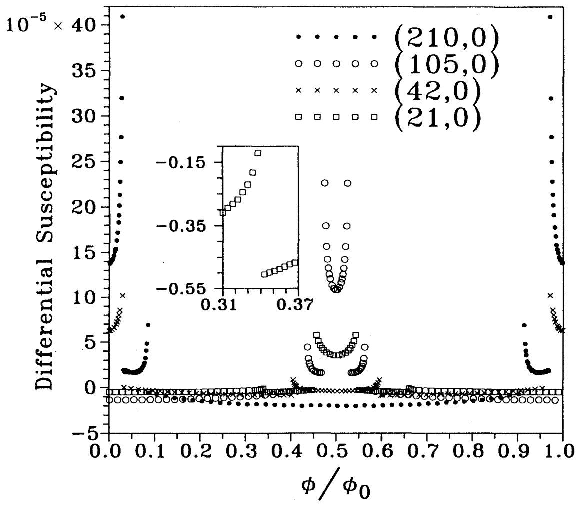

FIG. 16. The differential susceptibility comes from the magnetization shown in Fig. 15. The inset shows the details around the discontinuously sharp peak of the (21,0) tubule at $\phi\sim 0.34\phi_0$.

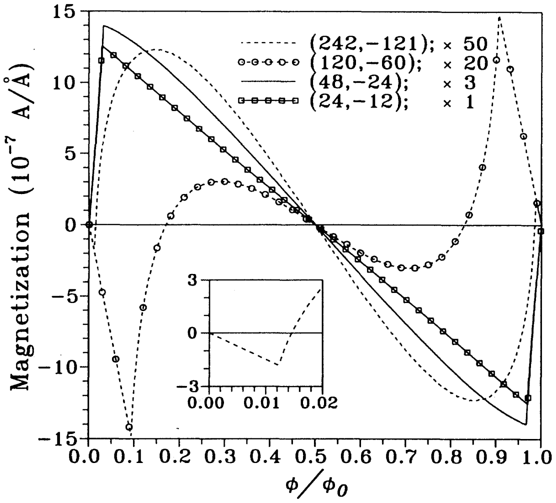

FIG. 17. Same plot as Fig. 15, but for the various armchair tubules with $(m,n)=(242,-121)$, $(120,-60)$, $(48,-24)$, and $(24,-12)$. The inset shows the details around the first cusp (or the magnetism transition) of the (242,21) tubule.

$M(\phi)$ is obviously affected by the chirality, which is contrary to the undoped case (see Fig. 5). However, for both zigzag and armchair tubules, the variation of the magnetization with ϕ (three kinds of behavior) is similar. For example, the magnetization of $(48,-24)$ and $(24,-12)$ tubules is paramagnetic, and quickly increases at small ϕ (the first kind), as seen in the (210,0) and (42,0) tubules. Here the two tubules $(120,-60)$ and $(242,-121)$ exhibit a special magnetism transition from diamagnetism to paramagnetism at small magnetic flux; i.e., their magnetization begins to decrease from zero, and then quickly rises to a positive value. This behavior belongs to the third kind of behavior. When the Fermi energy $E_F(0)$ is close to the lowest unoccupied conduction bands, the magnetization exhibits such behavior. Take the $(242,-121)$ tubule as an example. The two unoccupied conduction bands $J=91$ and 151 are very near to $E_F(0)$, and the energy difference E_D is -0.0003 eV. Only the $J=91$ subband becomes occupied at $\phi\geq 0.0146\phi_0$, and it makes a large and positive contribution to the magnetization. Therefore, a positively sharp rise is shown in M, and it leads to a special magnetism transition. It is noted that the doped zigzag tubule could also exhibit this kind of behavior (not shown), if its Fermi energy corresponds to that stated above. Basically, the variation of the magnetization with magnetic flux is very sensitive to the Fermi energy.

The magnetism at small flux deserves a closer examination. The Fermi energy $[E_F(0)]$ or the free-carrier density could be altered by introducing various intercalants into graphene tubules, as was done for GIC's.[12] The relation between magnetization and Fermi energy at $\phi=10^{-3}\phi_0$ is shown in Fig. 18 for the (210,0) tubule (open circles). The sharp increases in magnetization from negative to positive values occur at certain Fermi energies, where they are just above the highest occupied conduction bands (also see Fig. 11). The magnetization is in the same (opposite) direction as the external B field, if the

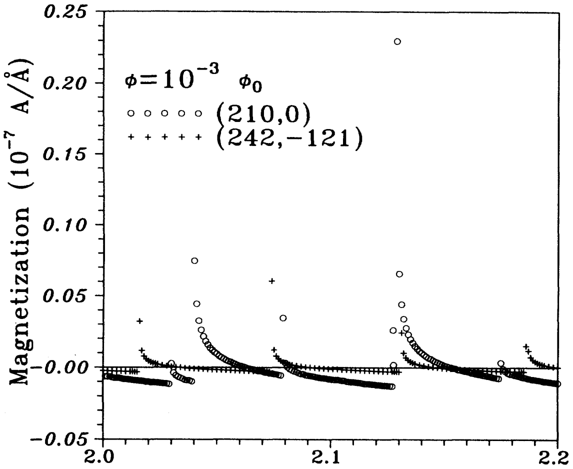

FIG. 18. The relation between magnetization and Fermi energy is plotted for the (210,0) tubule at $\phi=10^{-3}\phi_0$. The open circles and the plusses are those of the (210,0) and (242,−121) tubules, respectively.

introduced intercalants could bring the Fermi level close to the bottom of the highest occupied (lowest unoccupied) conduction bands; i.e., the doped tubule is paramagnetic (diamagnetic) under such a condition. Moreover, the special structures shown in M and χ_M occur at small flux. A similar relation between the magnetization and Fermi energy also exists in the armchair tubule (242,−121) (pluses), and so the feature is independent of the chirality. Although the tubule used in this study has $2m+n=3\times$integer, a similar feature (not shown) is obtained for another kind of tubule with $2m+n\neq3\times$integer. Hence the magnetism of the graphene tubule is possibly changed by introducing various intercalants, and it depends on the Fermi energy (or free-carrier density) and electronic structure. This feature is apparently different from that of the undoped tubule, because the undoped tubule with $2m+n=3\times$integer ($\neq3\times$integer) must be paramagnetic (diamagnetic) at small flux. The doping effects on the magnetism here are similar to those found between graphite (diamagnetism) (Ref. 27) and GIC's (Refs. 12 and 26) (the magnetism also depends on E_F).

V. CONCLUDING REMARKS

The magnetization and differential susceptibility of a graphene tubule with any chiral angle is studied in this work. There are cusps in $M(\phi,T=0)$ and power divergencies in $\chi_M(\phi,T=0)$ as a result of the spin-B interaction. The special structures shown in M and χ_M are insensitive to the chiral angle (for tubules with the nearly same radii). The temperature effect in reducing the magnetization is relatively obvious for a larger semiconducting tubule because of the smaller energy gap. Furthermore, an anomalous temperature effect is found to exist in a metallic tubule at relatively low temperature. For the doped graphene tubule, the magnetic properties strongly depend on the Fermi energy (or the free-carrier density) in addition to the geometric structure (including the radius and chiral angle).

The spin-B interaction is important in a graphene tubule, although its magnitude is small. It causes Zeeman splitting for the two spins, and makes the 1D subband capable of crossing the Fermi level at the flux ϕ_c before the parabolic dispersion of the crossing subband (J_a) becomes linear. The subband splitting destroys the periodicity (period ϕ_0) of the physical properties, and the divergent DOS of the crossing subbands results in cusps in $M(\phi,T=0)$ and power divergencies in $\chi_M(\phi,T=0)$. The power divergencies in χ_M are expected to be replaced by the peak structures at low temperature $T\leq1$ K. Moreover, the anomalous variation of M with T is caused by the spin-B interaction. The magnetic susceptibility in a graphene tubule is $10-10^2$ times larger than that of a metallic ring;[18–22] hence the anomalous features due to the spin-B interaction should be observable in the magnetic measurements. In addition, the spin-B interaction could lead to step structures in the ballistic magnetoconductance,[24] and the divergent structures (in $1/\sqrt{T}$ form) in the heat capacity.[25] In short, the importance of this paramagnetic interaction could be verified from the measurements of magnetization, magnetoconductance, and heat capacity.

The doping effects on the magnetic properties are summarized as follows. The Fermi energy here is very sensitive to the variation of the magnetic flux, but it always remains zero in the undoped case. The magnetization exhibits cusps even without spin-B interaction; moreover, the doping alters the number and the positions of the cusps in the presence of the spin-B interaction. The special structures, such as discontinuously sharp peaks, shown in the susceptibility are related to $[\partial^2E_F(\phi)/\partial^2\phi]^{1/2}$, and those of the undoped tubule belong to the power or logarithmic divergencies. The magnitude of the magnetic response could be increased by the doping, and so it is relatively easy to observe the special structures shown in M and χ_M for the doped tubule. The magnetic response is relatively strong for the larger doped tubules, but it hardly relies on the radii for the undoped tubules. If the undoped (m,n) tubule has $2m+n=3\times$integer ($\neq3\times$integer), it is paramagnetic (diamagnetic) at the small flux. However, the magnetism of the doped tubule may be paramagnetic or diamagnetic, and it is closely related to the energy difference between the Fermi level and the bottom of the highest occupied (or the lowest unoccupied) conduction band. Various intercalants could be introduced into the graphene tubule to alter the Fermi energy (or free-carrier density), as done for GIC's.[12] Therefore, the magnetism is possibly changed by the doping. The doping effects on the magnetic properties are expected to remain similar for a more complicated system, an n-layer coaxial tubule.

ACKNOWLEDGMENTS

One of us (M.F.L.) thanks Dr. Ya-Chi Tsai for a critical reading of the manuscript. This work was supported in part by the National Science Council of Taiwan, the Republic of China under the Grants Nos. NSC 83-0208-M-007-041 and NSC 84-2112-M-007-018.

[1] S. Iijima, Nature **354**, 56 (1991).

[2] S. Iijima, P. M. Ajayan, and T. Ichihashi, Phys. Rev. Lett **69**, 3100 (1992); S. Iijima and T. Ichihashi, Nature **363**, 603 (1993).

[3] C. H. Kiang, W. A. Goddard III, R. Beyers, J. R. Salem, and D. S. Bethune, J. Phys. Chem. **98**, 6612 (1994).

[4] J. W. Mintwire, B. I. Dunlap, and C. T. White, Phys. Rev. Lett. **68**, 631 (1992); C. T. White, D. H. Robertson, and J. W. Mintwire, Phys. Rev. B **47**, 5485 (1993).

[5] N. Hamada, S. I. Sawada, and A. Oshiyama, Phys. Rev. Lett. **68**, 1579 (1992).

[6] R. Saito, M. Fujita, G. Dresselhaus, and M. S. Dresselhaus, Appl. Phys. Lett. **60**, 2204 (1992); Phys. Rev. B **46**, 1804 (1992).

[7] R. A. Jishi, M. S. Dresselhaus, and G. Dresselhaus, Phys. Rev. B **47**, 16 671 (1993); R. A. Jishi and M. S. Dresselhaus, *ibid.* **45**, 11 305 (1992); R. A. Jishi, D. Inomata, K. Nakao, M. S. Dresselhaus, and G. Dresselhaus, J. Phys. Soc. Jpn. **63**, 2252 (1994).

[8] H. Ajiki and T. Ando, J. Phys. Soc. Jpn. **62**, 1255 (1993); **62**, 2470 (1993).

[9] M. F. Lin and K. W.-K. Shung, Phys. Rev. B **48**, 5567 (1993); **47**, 6617 (1993); Chin. J. Phys. **32**, 879 (1994).

[10] O. Zhou, R. M. Fleming, D. W. Murphy, C. H. Chen, R. C. Haddon, A. P. Ramirez, and S. H. Glarum, Science **263**, 1744 (1994).

[11] P. R. Wallace, Phys. Rev. **71**, 622 (1947).

[12] M. S. Dresselhaus and G. Dresselhaus, Adv. Phys. **30**, 139 (1981).

[13] M. S. Dresselhaus, *Intercalation in Layered Materials* (Plenum, New York, 1987).

[14] O. Zhou, J. E. Fischer, N. Coustel, S. Kycia, Q. Zhu, A. R. McGhie, W. J. Romannow, J. P. McCauley, Jr., A. B Smith III, and D. E. Cox, Nature **351**, 462 (1991).

[15] K. W.-K. Shung, Phys. Rev. B **34**, 979 (1986); M. F. Lin and K. W.-K. Shung, *ibid.* **46**, 12 656 (1992).

[16] G. L. Doll, M. H. Yang, and P. C. Eklund, Phys. Rev. B **35**, 9790 (1987); D. M. Hoffman, R. E. Heinz, G. L. Doll, and P. C. Eklund, *ibid.* **32**, 1278 (1985).

[17] P. Alstrom, Synth. Metals **15**, 311 (1986).

[18] L. P. Levy, G. Dolan, J. Dunsmuir, and H. Bouchiat, Phys. Rev. Lett. **64**, 2074 (1990).

[19] V. Chandrasekhar, R. A. Webb, M. J. Brady, M. B. Ketcham, W. J. Gallagher, and A. Kleinsasser, Phys. Rev. Lett. **64**, 3578 (1991).

[20] D. Mailly, C. Chapelier, and A. Benoit, Phys. Rev. Lett. **70**, 2020 (1993).

[21] D. Loss, P. Goldbart, and A. V. Balatsky, Phys. Rev. Lett. **37**, 1655 (1990).

[22] H. F. Cheung, Y. Gefen, E. R. Riedel, and W. H. Shih, Phys. Rev. B **37**, 6050 (1988).

[23] M. F. Lin and K. W.-L. Shung, Phys. Rev. B **50**, 17 744 (1994).

[24] M. F. Lin and K. W.-K. Shung, Phys. Rev. B **51**, 7592 (1995).

[25] M. F. Lin and K. W.-K. Shung (unpublished).

[26] F. J. DiSalvo, S. A. Safran, R. C. Haddon, J. V. Waszczak, and J. E. Fischer, Phys. Rev. B **20**, 4883 (1979); S. A. Safran and F. J. DiSalvo, *ibid.* **20**, 4889 (1979).

[27] N. Ganguli and K.S. Krishnan, Proc. R. Soc. London Ser. A **117**, 168 (1941).